IEEE Access
Multidisciplinary ⋮ Rapid Review ⋮ Open Access Journal

Received 30 September 2022, accepted 19 November 2022, date of publication 24 November 2022,
date of current version 30 November 2022.

Digital Object Identifier 10.1109/ACCESS.2022.3224575

RESEARCH ARTICLE

Variable Stiffness Pad and Its Application to Hybrid Rigid-Soft Robots

PHONGSAEN PITAKWATCHARA AND JETNIPIT ARUNRAT
Department of Mechanical Engineering, Faculty of Engineering, Chulalongkorn University, Bangkok 10330, Thailand
Corresponding author: Phongsaen Pitakwatchara (phongsaen@gmail.com)

This work was supported in part by the Faculty of Engineering, Chulalongkorn University.

ABSTRACT Robot manipulation can easily become unstable when interacting with stiff environment. This is due to high contact stiffness, which is usually cannot be controlled. Contact stiffness is an important factor for the robot to perform the tasks successfully. It helps determining the contact force, which in turn affects the robot response and stability of the interaction. To resolve this fatal shortcoming, we have developed the variable stiffness pad (VSP) and its pressure supply system, which can be integrated to typical rigid robots. It allows one to modify the contact stiffness appropriately for the task and environment at hand. By the controlled pressured of 0-100 kPa, the prototype VSP attached to a rigid gripper can vary its stiffness linearly in the range of 23.5-42.0 kN/m during contact with time constant of 130 ms. This unique feature is used to modify contact stiffness properly. Moreover, contact stress is reduced since the effective contact area is enlarged thanks to the adaptation of the VSP local contact surface to the object. A concept of *hybrid robots*, where several VSPs are installed at the interaction surface of rigid robot, is proposed. Unlike traditional robots, both *manipulation impedance* and *contact impedance* of the hybrid robot may be adjusted in order to interact with unstructured environment properly. Analysis and experiments show that the hybrid rigid-soft gripper can manipulate objects with different shapes and stiffness safely.

INDEX TERMS Variable stiffness pad, soft robot applications, hybrid robots, contact stability, impedance control.

I. INTRODUCTION

Currently, soft robots have received a wide interest as a new generation of robots to work in unstructured environment. Purely soft robots are inherently safe to interact with any environment due to their high structural compliance. Therefore, researchers have employed soft robots in manipulation because the compliance mitigates the impact force and allows the robot to adapt itself to the environment safely. For instance, [1] designed a continuum manipulator that can bend and stretch by employing a set of McKibben actuators inside the double helical weaved plastic mesh sheath. Bending motion may also be obtained using channels of pneumatic networks [2] or strain limiting layer [3]. A soft multiple segments robot arm [4] was controlled by pneumatic to track desired curvature approximated by piecewise constant curvature and rigid robot model. [5], [6] were examples of the soft light inflatable arms that can bear large/small payload by operating at high/low pressure. Nevertheless, the control is quite difficult and problematic [7], [8], [9].

Problems in actuation, sensing, and control were mentioned in many works. Specifically, controlling purely soft robots are extremely difficult since they are infinite dimensional systems. However, widely adopted constant curvature assumption [4], [10] for finite low-dimensional approximated model may incur error since purely soft robot interacting behavior is highly nonlinear. Worse yet, sensing and actuation are limited by current technology. Most sensor and actuator systems available are sparsely distributed, unwieldy, and non-collocated. Due to softness of the robots, sensing information and transmitting power are further deteriorated. These make designing and controlling soft robots even more difficult.

To overcome the problems, many robots were constructed from both soft and rigid components. For example, [11]

The associate editor coordinating the review of this manuscript and approving it for publication was Gerardo Flores.

designed a robot arm composed of a lightweight carbon fiber composite tubes, plastic joints, pneumatic artificial muscles, and inflatable sleeves as soft cushion. Compliant variable stiffness link [12] was developed and combined with the rigid links and joints to build a safe robot arm. Soft-bubble [13], a variable compliant and geometry gripper with integrated visuotactile sensor, was installed at the end-effector to grasp household objects.

The notion of covering rigid robots with soft materials has been introduced with different purposes. Soft inflatable tactile sensing sheet [14], having embedded microchannels with liquid metal inside, was wrapped around the plastic bone structure of the robot arm to provide tactile information for retraction behavior. Distributed magnetic field sensors were embedded into the skin [15] so that interaction force can be measured. CoboSkin [16] was a soft skin with distributed sensing and inflatable units. It is capable of reducing the impact force and measuring distributed contact force using foam sensors. In [17], contact force at the soft pad module was predicted from the light reflecting pattern detected by embedded optical sensors using neural network. Shape transformation of soft composite materials has also been leveraged in the area of human computer interaction [18], [19], [20]. Recently, a variable stiffness electroadhesion [21] was developed to lift and move curved and flat objects. Moreover, industries have already adopted soft skin idea, either in part [23] or as a whole [24], as a practical means for the collaborative robots.

Soft robotic technology has also been applied to modulate robot stiffness or compliance in various ways. For example, [12] varied stiffness of robot link by pressurizing the silicone-made cylindrical chamber that also serves as the robot link. In contrast, a tendon-tensioning control method [22] was used to change the stiffness of the backboneless segmented soft robot. Soft bubble gripper [13] can vary grasping force of the gripper through regulated pressure, in which linear relationship between the stiffness and the pressure was inferred. CoboSkin [16] unit was able to adjust its stiffness by internal air pressure. It was used to reduce peak impact force. Recently, [25] developed a robot palm using particle jamming technique and positive/negative pressurized chambers to control its stiffness and deformation. Finite element method was used to analyze the influences of regulated pressure, as well as the shape and size of cavities, on the stiffness of a Pneu-Net with particle jamming soft actuator [26]. These works focus on the control of stiffness variation. However, its aspect on the manipulation has not been mentioned.

It is well known that conventional rigid robots may easily become unstable during contact with stiff environment [27], [28], [29]. However, they can perform the tasks very well if the environmental states and parameters are precisely known, which is unlikely the case in practice. On the other hand, although purely soft robots are safe to interact with any environment, it is challenging to perform the tasks efficiently due to their compliance. According to these pros and cons, we propose a concept of *hybrid robots* that inherit the best part of purely soft and rigid robots. The robot core structure is built from rigid links, as commonly does in the rigid robot, in order that the tasks can be performed efficiently. At its surface, we develop the variable stiffness pad (VSP) as an inherently compliant robot skin installed at various locations where the interaction might happen. Its stiffness and possibly damping parameters are adjustable such that suitable contact impedance to the task at hand is realized. With proper movement and contact stiffness by the motion controller of rigid robot and the stiffness controller of the VSP, a range of interactive tasks may be accomplished. Figure 1 illustrates a conceptual hybrid humanoid robot interacting with several objects and environment at different parts simultaneously. With the VSP system, exhaustive motion planning during the task is unnecessary because the soft covered robot can unintentionally bump into the environment and react safely just like human does. Installation and working principle of the VSP are described in section II-B and III.

FIGURE 1. Illustration of the hybrid robot built from rigid links and VSPs (pink colored). The VSPs are installed at its feet, knees, elbows, and palms. These are body parts which frequently interact with unknown objects and environment.

Contributions of this paper are threefold.

- We present an apparatus consisting of a semi-active soft pad called the VSP and its pressure supply system. The prototype is installed to a rigid gripper as a demonstration of hybrid robot that allows one to modulate both manipulation and contact impedance. Therefore, the robot can manipulate a variety of unstructured objects efficiently and safely.
- We propose an interaction control structure consisting of manipulation impedance controller for the rigid robot, and contact impedance controller for the VSP. The latter is achieved through regulating the pressure inside a closed volume. Interaction dynamics and contact stability are analyzed. It is shown by simulation and experiments that the VSP helps improve contact stability during task execution. A guideline for adjusting suitable impedance parameter values is provided.

- The developed hybrid gripper prototype is a *multi-energy-domain system* [30] consisting of thermo-fluid system of the pressure supply unit, mechanical system of the rigid gripper, and continuum elastic/dissipative system of the VSP. We model these subsystems based on simplified lumped system modeling, various empirical experiments, and system identification techniques. These models are combined with causality consistency and used in controlling the hybrid gripper to grasp objects with different shapes and stiffness successfully.

Merits of applying the VSP to rigid robots may be summarized here.

- VSP allows one to modulate contact impedance apart from manipulation impedance. This supplement plays a vital role in interacting with the environment successfully.
- VSP improves contact stability during task execution. Only manipulation impedance may not be enough, especially when fast contact is made or the environment is stiff.
- VSP stores and absorbs surplus energy transferred from the robot to the environment, or vice versa. This is useful particularly for the tasks involving large impact force.
- VSP eliminates the need to know of true contact location used in the impedance control law.
- Soft VSP can tolerate uncertainties in the manipulation with stiff environment. Stiff VSP can improve responsiveness of the manipulation with soft environment.

Explanation of each item will be given in the upcoming context.

The paper is organized as follow. Section II introduces the VSP, its elastic model, and stiffness. Customized pressure supply system to control stiffness of the VSP is described in section III. Section IV proposes an interaction control structure and analyzes interaction dynamics and contact stability for the hybrid gripper. Experiments are presented in section V. Finally, section VI concludes the paper.

II. VARIABLE STIFFNESS PAD

Soft covers with fixed compliant characteristics [23], [24] may be installed at the robot contact surface to stabilize the interaction. However, there are tasks which simply cannot be accomplished without proper contact impedance. For instance, a humanoid robot will fail to run on a new terrain of different hardness if the foot contact impedance is not adapted accordingly. This inspires us to develop the VSP (Fig. 2i) which is a pad that can change its stiffness. The pad is semi-active in the sense that it has very small deformation associated with the stiffness adjustment. This is caused by inflation of the chamber and hence should not be treated as purposeful motion. When installed at the robot interaction port, the VSP can be used to modulate the *contact stiffness* properly; thus enabling the robot to perform a variety of tasks with different environments safely.

Several underlying physics may potentially be exploited in order to change the stiffness of the compliant materials. Shape memory alloys or polymers can change their shape by the induced temperature [31], [32]. Electroactive polymers expand and thus their stiffness change due to the supplied voltage [10], [33]. Obviously, elastomer-maded chambers inflate and stiffen according to the pressurized fluid inside [34]. Actuation of these soft materials has been studied widely for manipulating or locomoting soft robots. Nevertheless, their stiffness characterization does not receive much attention. Since we are interested in regulating the stiffness of the VSP, not the motion per se, relationship between the applied force and deformation across the compliant element against the stiffness controlled variable will be determined.

A. DESIGN

Our VSP is based on the elastomer chamber technology made from the RA-40AB silicone with the following key properties provided by the local manufacturer (RUNGART): Shore hardness 40A, tear strength 27 N/mm, tensile strength 6 MPa, and elongation at break 350%. The prototype for attaching to a gripper (see section V) has a footprint of $5 \times 5\,\text{cm}^2$ with 2 cm thick when not pressurized. Its air chamber is constructed from a few cylindrical vessels connected together to a common air conduit. Each vessel is made of the fabric-reinforced silicone. We use 3 vessels arranging in a row for the prototype. This layout helps increase the stiffness of the VSP as the vessels will act like springs connected in parallel. They are sandwiched between the fiber-reinforced silicone pads. When pressurized, the pressure force stiffens and thickens the VSP such that the pads are displaced apart at 1 mm *without swelling* for the maximum supplied pressure of 100 kPa or 1 bar and no externally applied force.

B. FABRICATION

Figure 2 displays the process in fabricating the VSP. First, we prepare mold half and the cylindrical vessel shaped rod by a 3D printer. They are assembled. Then, the uncured silicone is poured into the gap between the inner and outer molds. After curing at the room temperature, the innermost layer of a cylindrical vessel chamber is formed (Fig. 2a). Next, we wrap it with a sheet of finely non-woven spunbond polypropylene fabric (30 gsm) as the middle layer to limit the expansion of the pressurized vessel. Put this in another mold half and pour the silicone for the outermost layer coating the fabric (Fig. 2b). We trim the ends of the fabric to fit the vessel body (Fig. 2c).

Three finished cylindrical vessels are pushed fitted onto the hollow spurs of the 3D-printed base of the VSP, which serves as the air manifold to each vessel (Fig. 2d). They are secured together before casting on with thick silicone (Fig. 2e). Next, the air chamber unit is joined with the 3D-printed backplate, also serving as the basin mold, by the cured silicone in between (Fig. 2f). The backplate is used to fasten the VSP to the robot. Finally, the front pad is fabricated and joined by placing the unit on the front basin mold filled with the

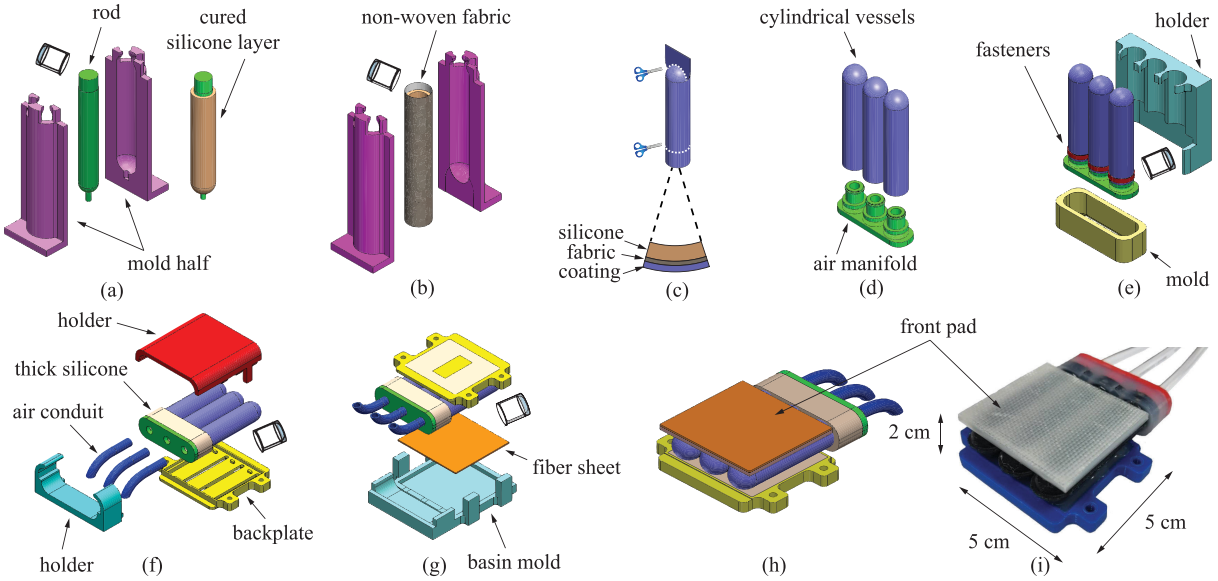

FIGURE 2. Fabrication process of the VSP.

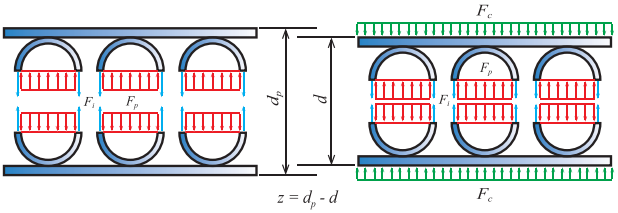

FIGURE 3. Cross sectional free body diagram of the VSP viewing along the cylindrical vessels when uncompressed (left) and compressed (right).

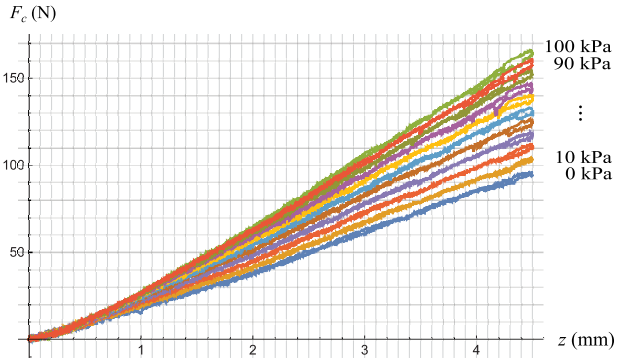

FIGURE 4. Contact force vs. deformation of the VSP at different pressure values.

uncured fiber-reinforced silicone (silicone with a sheet of 800 g/m^2 woven fiberglass embedded, Fig. 2g). After curing, the unit and the front pad are bonded. The finished VSP is obtained. Figure 2h and Fig. 2i show the CAD-rendered and the actual VSP.

C. MODELING AND CHARACTERIZATION

Figure 3 is the cross sectional free body diagram of the VSP revealing three major forces acting along the normal direction of the pad surface. They are contact force F_c distributed throughout the whole area of the pad, pressure force F_p developed from the pressure p inside the vessels, and pretension force F_i induced in the silicone membrane. When the VSP does not subject to F_c, its thickness d is the nominal value denoted as d_p. The compressed distance is thus $z = d_p - d$.

In order to control the stiffness of the VSP, we need to determine its elastic behavior which is described by the relationship between F_c, z, and p. For this matter, the VSP system is installed to the ball screw unit as shown in Fig. 14. The unit is driven at 1 mm/s to compress the VSP against the rigid wall.

At each p, first d_p is measured. Then the VSP is compressed over a working range of 4.5 mm while F_c and position of the VSP are sampled at 2 kHz. Corresponding value of z is determined. After that, p is changed to a new value over the entire range of operation and the compression step is repeated. The whole experiment is repeated 10 times to reduce data variance. Mean values are determined. Fig. 4 is a family of curves showing how the contact force varies as we pressurize and compress the VSP. Small hysteresis is observed at large z due to creeping behavior of the silicone at large deformation. Elastic model of the VSP is therefore determined.

D. STIFFNESS OF VSP

Stiffness of the VSP is defined

$$k_s(z, p) \triangleq \frac{\partial F_c(z, p)}{\partial z} \tag{1}$$

as the ratio of the change of the contact force to the change of the compressed distance, or the slope of F_c-z curve, at a specific pressure. To determine k_s, we first determine empirical equations for the curves in Fig. 4. It is observed that the

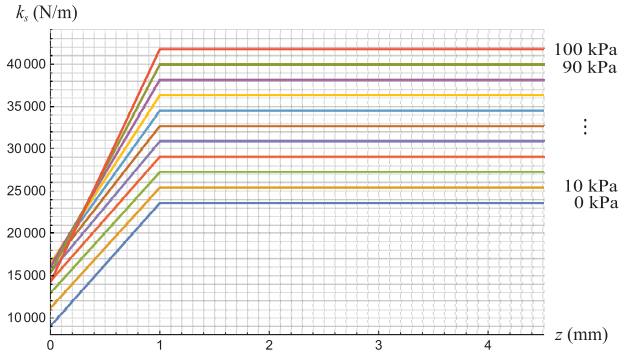

FIGURE 5. Stiffness variation of the VSP.

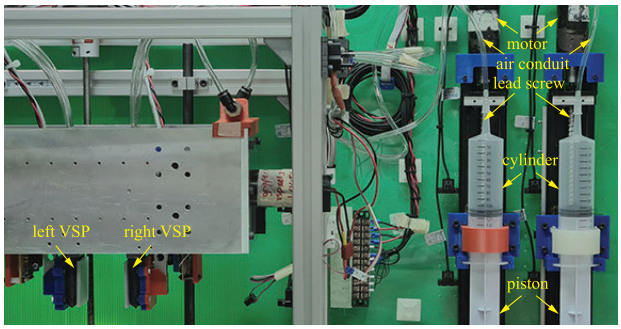

FIGURE 6. Air compressor unit equipped to the VSP.

trends of the curves F_c during $0 \le z \le 1$ and $1 < z \le 4.5$ mm are quadratic and linear in z respectively. Thus, the equation form used should be split accordingly. Based on optimal least square error criteria, the equations are determined as

$$F_c(z,p) = \begin{cases} a(p)z^2 + b(p)z, & 0 \le z \le 1 \\ k(p)(z-1) + c(p), & 1 < z \le 4.5 \end{cases} \quad (2)$$

where $k(p) = 23.6{+}18.2\frac{p}{p_{\max}}$, $c(p) = -9(\frac{p}{p_{\max}})^2{+}20.7\frac{p}{p_{\max}}{+}16.3$, $a(p) = k(p) - c(p)$, $b(p) = 2c(p) - k(p)$, and $p_{\max} = 100$ kPa. The units for F_c, p, and z are N, Pa, and mm.

Therefore, stiffness may be determined by substituting (2) into (1). Figure 5 plots the derived k_s against z for each p. It is observed that, for each specific compressed distance z, there is a range of stiffness that the VSP can achieve by varying the pressure. Spring characteristic of the VSP is nonlinear during $z \le 1$ mm. However, spring becomes linear when $z > 1$ mm and stiffness becomes constant for a selected pressure value. In this region, stiffness in the fixed range of 23.5-42.0 N/mm is linearly proportional to the pressure of 0-100 kPa, regardless of the value of z.

III. PRESSURE SUPPLY SYSTEM

One may employ a standard pressure supply system involving pneumatic pump and regulating valve to stiffen up the VSP. However, the output pressure is quite noisy and the resolution, on order of 10^3 Pa, is too low for our purpose. We have developed a customized air compressor unit shown in Fig. 6. It uses a motor and lead screw to drive the piston inside the cylinder. The piston then compresses the air in the closed control volume connecting to the VSP to a desired pressure. In the following, model of the air compressor unit is derived. Then, a sliding mode controller which computes the piston driving force so that desired pressure is achieved will be designed.

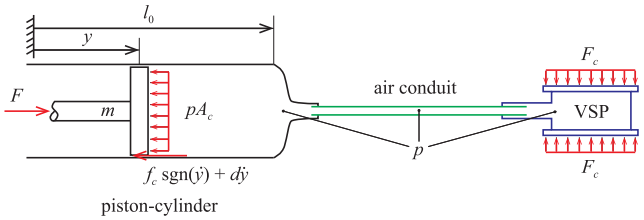

FIGURE 7. Schematic diagram of the pressure supply system and VSP.

A. MODELING OF AIR COMPRESSOR UNIT

Let A_c be the pressurized area of the piston normal to the cylindrical axis. The connecting motor, lead screw, and piston-cylinder of the air compressor unit may be modeled as an equivalent moving mass m subject to the driving force F, the resisting pressure force pA_c, and Coulomb plus viscous friction force appeared in the drivetrain and at the rubber plunger. Schematic diagram is depicted in Fig. 7.

Let y be the piston position measured from its starting point. Equation of motion becomes

$$m\ddot{y} + d\dot{y} + f_c\,\mathrm{sgn}(\dot{y}) + pA_c = F \quad (3)$$

in which f_c is the magnitude of Coulomb friction and d viscous damping coefficient. Values of f_c, m, and d may be estimated off-line. Let $\hat{\cdot}$ indicate the estimated quantity. After detaching the VSP from the air compressor unit which nullifies the pressure force for the moment, $\hat{f}_c = 9.47$ N is readily determined from the average of F that makes the piston start moving at different positions along the cylinder. Then the Coulomb friction is feedforward to F as $F = F_d + \hat{f}_c\,\mathrm{sgn}(\dot{y})$. In turn, (3) approximately becomes

$$m\ddot{y} + d\dot{y} = F_d \quad (4)$$

Equation (4) is integrated with respect to time and low-pass filtered by $\frac{\lambda_c}{s+\lambda_c}$ where s is the Laplace operator and λ_c the cut-off frequency. The result may be arranged as

$$y = \begin{bmatrix} \frac{\lambda_c}{s+\lambda_c}y & \frac{\lambda_c}{s+\lambda_c}\int F_d\,d\tau \end{bmatrix} \begin{bmatrix} 1 - \frac{d}{\lambda_c m} \\ \frac{1}{\lambda_c m} \end{bmatrix} \quad (5)$$

In order to estimate m and d, $F_d = A\sin\frac{2\pi t}{600}$ N, with the magnitude A decreasing from 50 N by 3 N step-wise at every 600 ms, is applied to the system for 6 seconds. The filter of $\lambda_c = 100$ rad/s is used. Output y and the filtered terms in (5) are sampled and evaluated at 1 kHz. Parameters $\hat{m} = 20.76$ kg and $\hat{d} = 180.7$ N·s/m are obtaied by solving for unknown column vector in the linear system generated from (5) that minimizes mean square error, using pseudoinverse.

When the air conduit of the cylinder is connected to the VSP, the closed chamber is formed. If the piston is compressed or retracted, gauge pressure p will then be increased or decreased. Assume the air inside is ideal gas and undergoes polytropic process involving heat transfer,

$$(p + p_a)V^n = \text{constant} \tag{6}$$

holds in which n is the polytropic index. If there is no heat transfer, the air indeed undergoes isentropic process and $n = \gamma = c_p/c_v = 1.4$ at 25°C [36]. For this system which has heat loss from the air compressor to the surroundings, $n = (1-\gamma)\frac{\delta Q}{\delta W} + \gamma$ where $\frac{\delta Q}{\delta W}$ is the rate of heat loss per work input [35]. By estimating efficiency of the process to be 0.6, $n = 1.24$ is adopted. Note that $p_a = 101.325$ kPa at 25°C.

Volume of the closed chamber V is determined from

$$V = V_0 + V_c + V_s. \tag{7}$$

in which $V_0 = 36\,\text{cm}^3$ is the volume inside the conduit circuit. $V_c \approx A_c(l_0 - y)\,\text{cm}^3$ is the volume inside the piston-cylinder, where $l_0 = 12.73$ cm is the available stroke length of the piston initially and $A_c = 12.57\,\text{cm}^2$. Volume of the VSP is estimated empirically as a function of its thickness, i.e. $V_s \approx V_s(d) = V_s(d_p - z) = 12.96(d_p - z - 1.0)^2\,\text{cm}^3$.

B. PRESSURE AND STIFFNESS CONTROLLER

Pressure at the cylinder and at the VSP may be approximately the same since the total volume (209 cm^3 nominally) is not substantial. It is controlled through the piston stroke y compressing the air inside. Therefore, gas law (6) is involved. However, the model might be imprecise due to permeability property of the silicone at large time scale. To improve the accuracy, (6) should be applied across small time interval $[t_1, t_2]$. Let t_1 be current time and t_2 be the time when desired pressure p_d is achieved. Associated piston position y_d, as a function of p_d, p, F_c, and y, may be determined from (6) and (7) as

$$y_d(p_d) = l_0 - \frac{1}{A_c}\left(\left[\frac{(p+p_a)V^n}{p_d + p_a}\right]^{\frac{1}{n}} - V_0 - V_s(d_{p_d} - z(F_c, p_d))\right) \tag{8}$$

Practically, simplified model of (3) and (6) have neglected complexity of actual system to an extent. Moreover, measured and estimated values are coupled with some errors. To address this issue, a proportional-integral pressure feedback may be used to correct for the reference value of y

$$y_r(p_d, p) = y_d(p_d) + K_p(p_d - p) + K_i\int(p_d - p)\,d\tau \tag{9}$$

that makes $p \to p_d$. The gains $K_p = 0.6 \times 10^{-3}$ and $K_i = 0.012 \times 10^{-3}$ are used.

Error in nonlinear plant (3) comes from modeling simplification and parameter uncertainties. With some knowledge about parameter error bounds, sliding mode control technique [37] may be employed to control y in (3) to follow y_r. Resulting system becomes robust and outperforms the use of conventional PID controller. Few works have applied this technique to regulate the pressure in soft robots, such as [38].

Let the parameter uncertainty bounds in (3) be $|\hat{m}-m| \le e_m$, $|\hat{d}-d| \le e_d$, $|\hat{f}_c - f_c| \le e_{f_c}$, $|\hat{A}_c - A_c| \le e_{A_c}$. Depending on the confidence level of estimated parameters, $e_m = 2.1$ kg, $e_d = 1.8\,\text{N}\cdot\text{s/m}$, $e_{f_c} = 2.5$ N, and $e_{A_c} = 40\,\text{mm}^2$ are chosen. Define $s \triangleq \dot{\tilde{y}} + \lambda\tilde{y} = 0$ be the sliding surface. Parameter λ is the tracking closed loop bandwidth and $\tilde{y} = y - y_r$ is the tracking error. One may devise a discontinuous control law based on the above modeling error such that $s \equiv 0$ is satisfied in finite time. However, the controller will excite unmodeled high frequency dynamics. This may be alleviated by setting an attractive boundary layer around $s = 0$, which is less aggressive requirement for tracking subject to modeling error. Moreover, the corrective stepwise force is linearly interpolated inside the boundary layer. Chattering is thus eliminated.

The boundary layer is defined as $\mathcal{S} = \{(y, \dot{y}) \mid |s| \le \Phi\}$ where Φ is the time-varying boundary layer thickness. Condition

$$\frac{1}{2}\frac{d}{dt}s^2 \le (\dot{\Phi} - \eta)|s| \tag{10}$$

when $|s| > \Phi$ must be satisfied for $\mathcal{S}$ to be attractive.

Differentiating s and applying (3), the driving force

$$F = \hat{m}(\ddot{y}_r - \lambda\dot{\tilde{y}}) + \hat{d}\dot{y} + \hat{f}_c\,\text{sgn}(\dot{y}) + p\hat{A}_c - \overline{k}\,\text{sat}(s/\Phi) \tag{11}$$

with control discontinuity gain

$$\overline{k} = e_m|\ddot{y}_r - \lambda\dot{\tilde{y}}| + e_d|\dot{y}| + e_{f_c} + pe_{A_c} + \mathfrak{m}(\eta - \dot{\Phi}) \tag{12}$$

and variable

$$\mathfrak{m} = \begin{cases} \hat{m} - e_m, & \eta - \dot{\Phi} < 0 \\ \hat{m} + e_m, & \eta - \dot{\Phi} \ge 0 \end{cases}$$

may be applied to the piston such that (10) is satisfied. Boundary layer thickness Φ is governed by

$$\dot{\Phi} = -\lambda\Phi + \frac{e_m|\ddot{y}_r| + e_d|\dot{y}_r| + e_{f_c} + pe_{A_c}}{\mathfrak{m}} + \eta \tag{13}$$

with $\Phi(0) = \left(\frac{e_m|\ddot{y}_r(0)| + e_d|\dot{y}_r(0)| + e_{f_c} + pe_{A_c}}{\hat{m} + e_m} + \eta\right)/\lambda$.

Stability of the closed loop system (3) and (11)-(13) may be deduced from (10) that the state is attracted to $\mathcal{S}$. Hence, magnitude of $\tilde{y}$ influenced by modeling error will be bound. This can be proven as follow. Substitute (11)-(12) into (3) and recall $m(\ddot{\tilde{y}} + \lambda\dot{\tilde{y}}) = m\dot{s}$. For $|s| > \Phi$, multiply $m\dot{s}$ by s and note that $\text{sat}(s/\Phi)s = \text{sgn}(s)\,s = |s|$. Since $\hat{m} - e_m \le m \le \hat{m} + e_m$, it can be shown after simplifying the terms that $ms\dot{s} \le m(\dot{\Phi} - \eta)|s|$, which is equivalent to (10). Therefore, $\mathcal{S}$ is attractive. Equation (13) results from setting the dynamics of s to be a first-order filter of bandwidth λ when $|s| \le \Phi$. This makes $\mathcal{S}$ be invariant. Consequently, $|s| \le \Phi$ implies $|\tilde{y}|$ is bound to Φ/λ in finite time.

Parameter $\eta = 2.4$ N is chosen to be small positive value compared to $e_m|\ddot{y}_r| + e_d|\dot{y}_r| + e_{f_c} + pe_{A_c}$, and $\lambda = 180$ rad/s is tuned to the largest possible value while $|s| \le \Phi(t)$, $\forall t$ is still satisfied. The control law (11) ensures the position

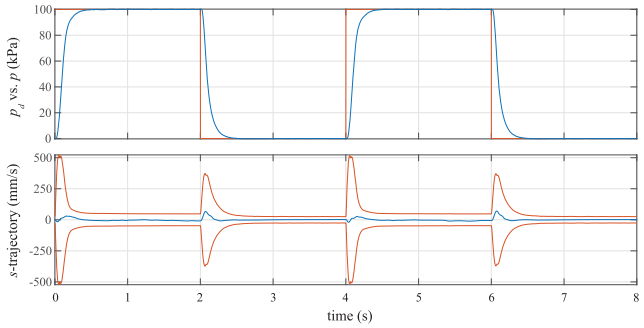

FIGURE 8. Desired (red) vs. actual (blue) pressure and *s*-trajectory (blue) residing in the uncertainty bound Φ (red) of the controlled air compressor unit subject to a pulse train of desired pressure at 100 kPa.

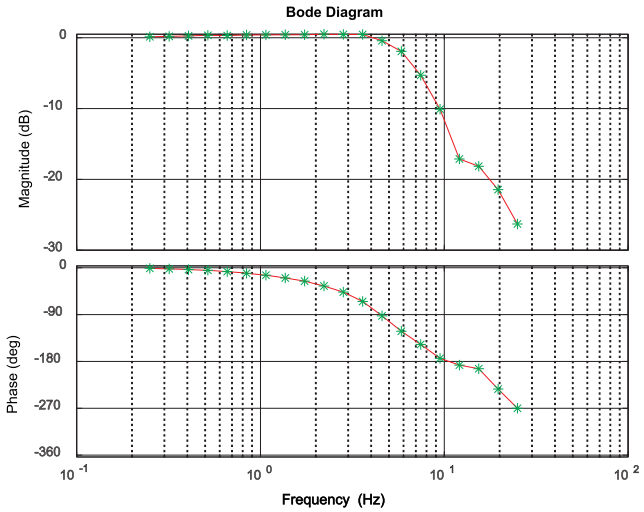

FIGURE 9. Frequency response of the developed pressure inside the VSP vs. desired pressure.

error $|\tilde{y}| \leq (\frac{e_m|\ddot{y}_r|+e_d|\dot{y}_r|+e_{f_c}+pe_{A_c}}{\mathrm{m}} + \eta)/\lambda^2$. In turn, p tracks p_d within a guaranteed precision, and hence desired stiffness of the VSP is achieved. Figure 8 depicts the pressure step response and corresponding *s*-trajectory of the controlled air compressor unit. It can supply the pressure in the range of 0-100 kPa with time constant of 130 ms and resolution of 8.6 Pa due to resolution of the motor encoder. Since s is bounded by Φ, p tracks p_d within a guaranteed precision (time-varying). Empirical pressure frequency response is plotted in Fig. 9. Cut-off frequency at -3 dB shows the developed VSP is capable of changing its stiffness dynamically up to 6 Hz.

At each sampling, contact force and pressure are measured. Then, compressed distance may be calculated from the inverse of (2). Given this and desired stiffness, corresponding pressure is determined from the inverse of (1). Therefore, stiffness may be controlled through regulating the supplied pressure. Note the resolution of the VSP stiffness during contact is 1.56 N/m, as computed from (2).

IV. INTERACTION CONTROL OF THE HYBRID GRIPPER

The prototype VSP is installed at a rigid gripper surface to create a hybrid rigid-soft gripper. Figure 10 shows the hybrid gripper interacting with the environment. According to physical layout of rigid gripper, VSP, and environment, we propose a low-level interaction control structure consisting of 1) impedance controller of the rigid gripper, which imposes *manipulation impedance* B and K, and 2) stiffness controller of the VSP, which imposes *contact impedance* b_c and k_c. Manipulation and contact impedance characterize motion response of the gripper subject to the resultant force, while contact impedance dictates contact force at the interaction port when the VSP and the environment are being compressed.

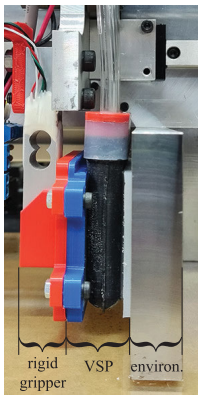

FIGURE 10. Physical layout of rigid structure and VSP of the hybrid gripper interacting with the environment.

A. CONTROL STRUCTURE

A typical passive impedance control law

$$F = B(\dot{x}_r - \dot{x}) + K(x_r - x) \tag{14}$$

attempts to drive robot motion $x, \dot{x}$ according to the reference $x_r, \dot{x}_r$ while shaping the manipulation stiffness and damping to K and B during free motion. It leaves the effective mass and robot friction intact.

When hybrid gripper is in contact with the environment, contact stiffness k_c denoting the change of contact force to the change of the VSP and environment deformation is established. Apparently from Fig. 10 and a simplified contact dynamic model in Fig. 11, it is determined from the combined stiffness of the VSP and the environment, k_s and k_e, in series as

$$k_c = \frac{k_s k_e}{k_s + k_e} \tag{15}$$

Equation (15) may be used to determine k_s that yields desired k_c for a specific k_e. Contact damping is formulated by the damping of the VSP and the environment in a similar manner. Overall hybrid gripper system is summarized in the diagram in Fig. 12.

B. INTERACTION DYNAMICS AND CONTACT STABILITY

Generally, manipulation dynamics are very complicated due to complex nature of the contact, friction force, impedance, and involved motion of the robot and environment. Nevertheless, for the impedance controlled hybrid gripper, we propose

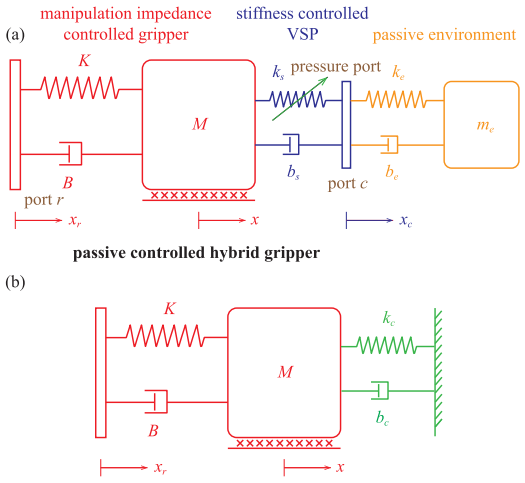

FIGURE 11. (a) Interaction model of the impedance controlled hybrid gripper in contact with the passive environment. (b) Simplified model in which the stiffness and damping of the VSP and static environment are combined.

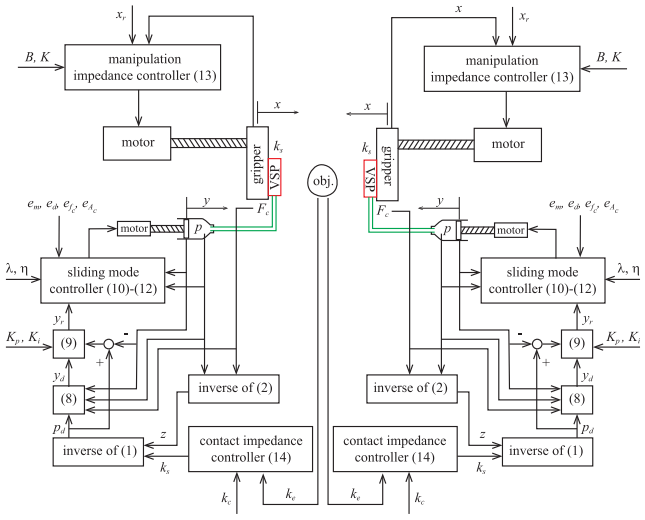

FIGURE 12. Diagram of the hybrid gripper system showing the hardware and the controllers.

a simplified model in Fig. 11a that captures the essence of its manipulation. It is a concatenation of the impedance controlled rigid gripper having desired parameters M, B, K, the stiffness controlled VSP with k_s and b_s, and the passive environment modeled as m_e, b_e, k_e. Intrinsic friction of the gripper drivetrain is not included in the model. Indeed, this helps improving stability of the contact we are considering.

Contact stability is defined as the ability of the gripper to maintain sudden contact with stiff environment. To analyze contact stability, the environment is immobilized as shown in Fig. 11b. This model well represents the tasks where the gripper exerts interaction force to the environment having no motion or moving with low speed.

Accordingly, motion of the gripper satisfies

$$M\ddot{x} + (B + b_c)\dot{x} + (K + k_c)x = B\dot{x}_r + Kx_r \tag{16}$$

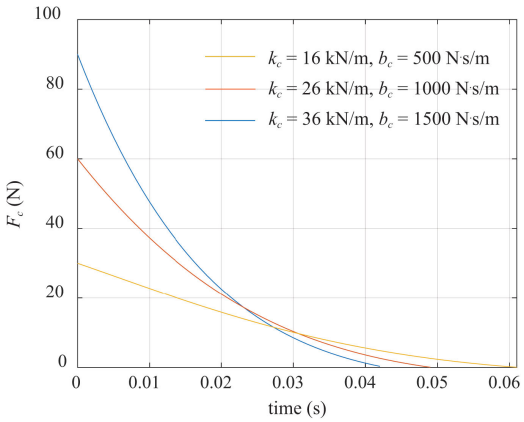

FIGURE 13. Evolution of interaction force when sudden contact is established until broken ($F_c = 0$).

while the interaction force

$$F_c = b_c\dot{x} + k_c x \tag{17}$$

must be positive during contact. If $F_c \leq 0$, contact is broken. At $x = 0$, the gripper starts contacting with the environment. To simulate sudden contact, let $x(0) = 0$ and $\dot{x}(0) = v_0 = 40\,\text{mm/s}$ due to initial kinetic energy. Moreover, to study the effect of contact impedance on contact stability, $x_r \equiv 0$ and $\dot{x}_r \equiv 0$ are set.

Assuming (16) is underdamped, its solution may be expressed as

$$x(t) = \frac{v_0}{\omega_d} e^{-\zeta\omega_n t} \sin \omega_d t \tag{18}$$

where $\omega_n = \sqrt{\frac{K+k_c}{M}}$, $\zeta = \frac{B+b_c}{2\sqrt{M(K+k_c)}}$, and $\omega_d = \omega_n\sqrt{1-\zeta^2}$. Performing parameter identification as done for the air compressor unit in section III-A, $\widehat{M} = 32.53\,\text{kg}$. Impedance parameters used in (14) are $K = 40\,\text{kN/m}$ and $B = 1.5\,\text{kN·s/m}$.

Substituting (18) and its derivative into (17), interaction force during contact may be determined. Plot of F_c vs. time as b_c and k_c vary is depicted in Fig. 13. It is seen that the peak of F_c occurs when contact is established. Larger b_c and k_c yield higher peak force. Also, the gripper tends to lose contact sooner as b_c and k_c become larger. In other words, low values of b_c and k_c improve contact stability. At the extreme with a rigid steel gripper, k_c becomes 7.65 MN/m. Initial contact force increases to 916 N (not plotted) and the contact is broken at $t = 7\,\text{ms}$ only. Therefore the stiffness, and byproduct damping, of the VSP may be lowered in order to improve stability of the contact.

C. STIFFNESS AND DAMPING SELECTION

Although the above analysis is done in the context of a gripper interacting with the object, it can be readily extended to general robot manipulation setting. From (16), impedance parameters M, $B + b_c$, and $K + k_c$ govern the robot motion during interaction. If B and K are large, x will track x_r closely for free motion. However, if they are too large, high

impact force and large steady-state force during contact may result. Likewise, by (17), large b_c yields high impact force while large k_c causes significant steady-state force. When both M and k_c are large, force and motion responses will be overshooting and oscillating since excessive kinetic energy is rapidly transformed into the spring potential energy, which then is quickly converted back again to kinetic energy reciprocally long before fully dampened out.

Usually, manipulation impedance values are selected according to the performing task and the environment. Nevertheless, there are lower bound for M and upper bounds for B and K, which prevent the system from instability due to quantization effect and limited actuation bandwidth. From (16)-(17) and contact stability, contact impedance should not be greater than manipulation impedance, or the manipulation would be dominated by the contact. If there is no special requirement, it is suggested that $b_c = B$ and $k_c = K$ in order for the robot to exercise enough interaction force promptly to the environment while not destabilizing motion and contact responses.

According to (15), the VSP is developed as a means to change stiff contact of the rigid robot and environment to a softer one with the value comparable to the manipulation impedance. Effectively, it acts as a medium that helps storing and absorbing surplus energy transferred from the robot to the environment. Soft VSP can store more energy at the slower rate than stiff VSP. Thus, the former should be employed to tolerate uncertainties in the manipulation with stiff environment that jeopardize contact stability severely. On the other hand, stiff VSP yields good force transparency so that it may be paired with soft environment to improve responsiveness of the manipulation.

Note that actual position and velocity feedback in (14) for hybrid robot belong to the point where the VSP is mounted to the robot. They may be computed from the robot kinematics readily. However, for rigid robot, they must be of the effective contact point between the robot and the environment. It is very difficult to acquire such values since for general tasks the contact point is not known a priori and subject to change. Exteroceptive sensors could be used but the result may not be precise enough. Employing the VSP thus eliminates the need to know of true contact location.

It should also be mentioned that the mechanism used to realize desired manipulation impedance and contact stiffness are different. Manipulation impedance is achieved through motor torque (14), in which B and K are rendered virtually. This is convenient but subject to low bandwidth limit caused by unwanted actuation dynamics. On the other hand, contact stiffness results from physical interaction with the elastic VSP and the pressurized air inside. Therefore, contact stiffness has no bandwidth limit. This is an important factor for the robot to perform demanding tasks successfully.

V. EXPERIMENTS

In order to illustrate the manipulation superiority of hybrid robot using the proposed VSP, experiments of the hybrid gripper interacting with different objects are performed. Accompanied videos are available in the multimedia attachment.

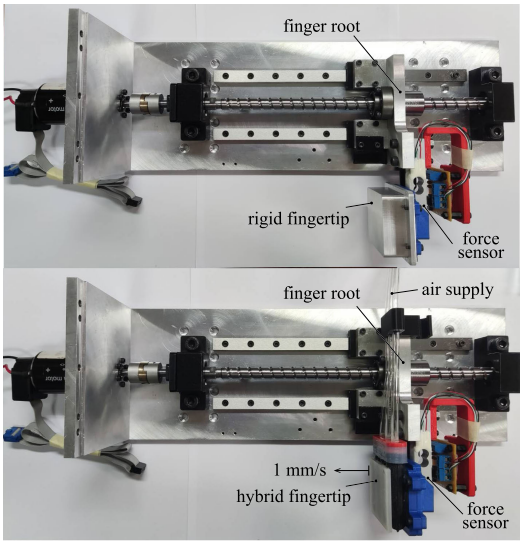

FIGURE 14. Rigid (top) and hybrid (bottom) finger unit.

A. EXPERIMENT SETUP

We have built a simple gripper with left and right fingers controlled separately. This may be viewed as two robots performing the task cooperatively. The gripper is designed with high rigidity and low backlash characteristics, while still backdrivable. Therefore, rigid structure of the finger is made of Aluminium alloy 7075-T6. Inside the structure between the root and the tip of the finger, a 1-DOF force sensor capable of withstanding 20 kg payload is installed. It is used to measure the contact force F_c which, together with the sensed pressure, can infer the compressed distance of the VSP in real-time.

The fingertip is designed to be interchangeable; user can choose either rigid or hybrid finger as shown in Fig. 14. Motion of each finger is driven by a MAXON DC motor (RE-148877) equipped with a 500 counts per turn encoder (HEDL-5540). This is converted into translational motion through an Oldham coupling and a ball screw with linear guide, having the stroke of 20 cm and the lead of 10 mm. Driving system of the air compressor unit is designed similarly.

An operational amplifier IC (INA128) is used to construct a circuit which amplifies very low output voltage signal from the force sensor's bridge circuit by 501 times. The motor is driven by its driver (ADS 50/10) in current drive mode. All sensor signals from encoders, force, and pressure sensors are sampled at 1 kHz using a PCIe interface analog/digital I/O board (Sensoray 826). The controller is implemented in C and run on a general desktop PC. Required driving forces are computed according to desired stiffness and force/motion. They are converted to output voltage signals and sent to respective motor drivers.

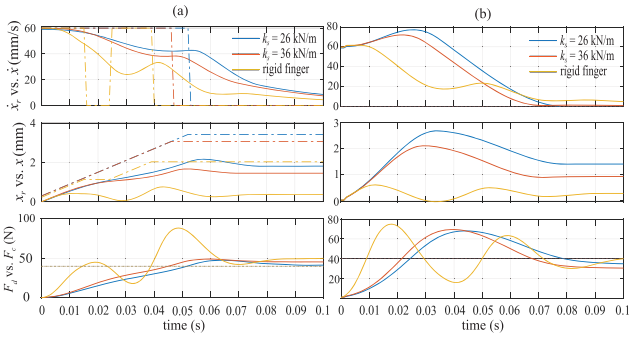

FIGURE 15. Reference (dashed line) vs. actual (solid line) velocity, position, and contact force during touching a rigid wall of three types of the finger using (a) impedance controller (b) force controller.

B. TOUCHING THE WALL

In this experiment, one of the two fingers of the gripper is controlled to touch a rigid wall with desired contact force $F_d = 40\,\text{N}$. Three types of the finger, i.e. hybrid finger with $k_s = 26$ and $36\,\text{kN/m}$, and rigid finger with a rigid pad, are employed. However, location of the wall is not known. Because of the rigid wall, k_c becomes 26, $36\,\text{kN/m}$, and a very large value with respective finger type during the touch. We apply (14) with $K = 40\,\text{kN/m}$ and $B = 1.5\,\text{kN}\cdot\text{s/m}$ for all fingers. Reference motion $\dot{x}_r$ is assigned based on actual contact force F_c as

$$\dot{x}_r = \begin{cases} \dot{x}_d, & F_c < F_d \\ 0, & F_c \geq F_d \end{cases} \tag{19}$$

where $\dot{x}_d = 60\,\text{mm/s}$.

Figure 15a displays $\dot{x}_r$ vs. $\dot{x}$, x_r vs. x, and F_d vs. F_c of each finger type at the touching moment during 100 ms time interval in order to examine the responses clearly. Initially, all finger types move toward the wall with the speed $\dot{x}_d$. When touching, rigid finger and the wall constitute a combination of large M and k_c with small b_c. This makes F_c overshoot and oscillate. On the other hand, the VSP of the hybrid finger reduces $k_c < K$ and increases b_c. Effectively, contact is stabilized as F_c slowly increases. The finger with $k_c = 36\,\text{N/mm}$ is more responsive than the one with $k_c = 26\,\text{N/mm}$. Due to conditions of $\dot{x}_r$ in (19), steady state value of F_c exceeds F_d for all fingers. The stiffer the finger is, the larger the contact force it creates.

For the rigid finger, $\dot{x}_r$ switches between 0 and $\dot{x}_d$ at $t = 16$, 25, and 40 ms due to oscillating F_c. Together, these $\dot{x}_r$ and F_c cause intermittently unstable contact which almost break apart at $t = 29\,\text{ms}$. This does not happen to the hybrid finger. Indeed, the VSP permits the rigid structure to move farther beyond the initial contact point at $x = 0$ while F_c gradually develops until F_d has reached. Softer VSP allows more compression than the harder one at the expense of more settling time. Therefore, unintentional contact is stabilized using the VSP, even with high impact speed. Desired interaction response may be achieved with proper contact and manipulation impedance.

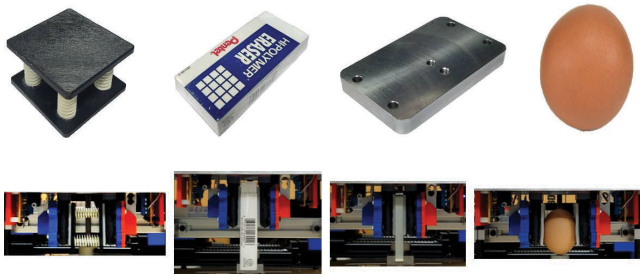

FIGURE 16. (Top) Various objects: a spring block, a pencil eraser, a finished steel plate, and a raw egg. (Bottom) Hybrid gripper grasping these objects.

The effect of using the VSP with force control is also studied. In this case, (14) is switched to a Proportional-Integral (PI) force controller

$$F = F_d + K_p(F_d - F_c) + K_i \int (F_d - F_c)\, d\tau \tag{20}$$

when $F_c \geq 1\,\text{N}$, i.e. after a slight touch with the wall. Controller gains are $K_p = 1$ and $K_i = 0.01$. Figure 15b compares the result alongside with the case when the impedance controller is used. Overall, force controller successfully regulates F_c to F_d at the price of more transient overshoot for all finger types. However, the VSP quickly damps out the oscillation. It also helps maintain sudden contact, i.e. contact is not lost for the hybrid finger. Therefore, the VSP may be applied to stabilize the interaction of the robot with unstructured environment, regardless of the controller used.

C. PICK AND PLACE THE OBJECTS

The above fingers are used to construct a simple gripper. Each type of gripper is used to pick up four objects: a spring block with stiffness $k_e = 20\,\text{kN/m}$, a pencil eraser, a finished steel plate, ranked in ascending order of stiffness, and a raw egg depcited in Fig. 16. Initially, the object is placed at some unknown location within the gripper stroke. Subtasks are to grip the object, pick it up, move to the left by 35 mm, place down, and release. Speed of the fingers during gripping and moving is set to be $\dot{x}_s = 40\,\text{mm/s}$. Suitable gripping force F_s of 20 and 40 N are required to grasp the egg and other objects firmly throughout the execution.

Parallel force-position controller described on pp. 381-384 in [39]

$$F = K_P C_F(F_d - F_c) + K_P(x_d - x) - K_D\dot{x} \tag{21}$$

is used to perform pick and place operation. It allows us to specify both F_d and x_d. In fact, (21) is the combination of force and impedance controllers. To compare the hybrid gripper with the rigid one, same controller parameters of $K_P = 15\,\text{kN/m}$, $K_D = 1.8\,\text{kN}\cdot\text{s/m}$, and $C_F = 0.3\,\text{m/kN}$ are used in every trial. We plan for F_d and $\dot{x}_d$ (speed) during major phases of the task as follow

$$\text{gripping:}\quad F_d, \dot{x}_d = \begin{cases} 0, \dot{x}_s, & F_c < F_c^* \\ F_s, 0, & F_c \geq F_c^* \end{cases}$$

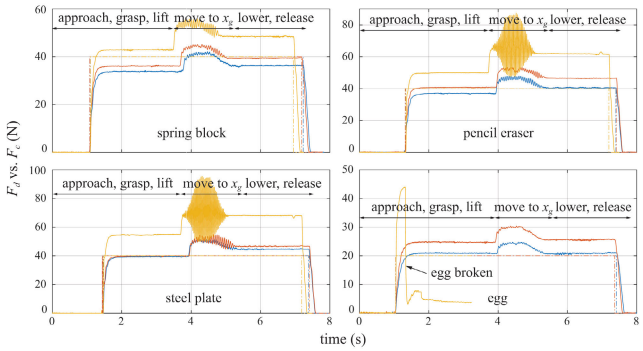

FIGURE 17. Desired (dashed line) vs. actual (solid line) gripping force of 3 grippers' right finger picking up 4 objects. The grippers are hybrid gripper with $k_s = 26$ (blue), 36 (red) N/mm, and the rigid gripper (yellow).

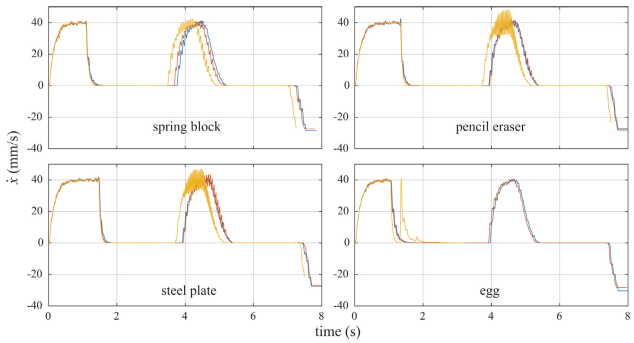

FIGURE 18. Actual velocity of 3 grippers' right finger picking up 4 objects. The grippers are hybrid gripper with $k_s = 26$ (blue), 36 (red) N/mm, and the rigid gripper (yellow).

$$\text{moving:}\quad F_d, \dot{x}_d = \begin{cases} F_s, \dot{x}_s, & x_g - x > g \\ F_s, \dfrac{x_g - x}{g}\dot{x}_s, & x_g - x \le g \end{cases}$$
$$\text{releasing:}\ F_d, \dot{x}_d = 0,\ \dot{x}_s \qquad (22)$$

where $F_c^* = 1$ N is the threshold used to determine whether the finger touches the object or not. Goal position of the object relative to the gripping location is $x_g = 35$ mm. When the object is far from the goal than $g = 10$ mm, $\dot{x}_d = \dot{x}_s$. As it moves past g, $\dot{x}_d$ is reduced to 0 proportionally in order to slow down and stop the motion.

Figure 17 and 18 compare F_c and $\dot{x}$ of different grippers manipulating objects. For the spring block, contact stiffness of the hybrid gripper with $k_s = 26$, 36 kN/m and the rigid gripper are $k_c = 11.3$, 12.9, and 20 kN/m respectively. The latter yields the largest F_c from the smallest compression of the grasping. During object movement, F_c chatters due to speed mismatch, oscillating out of phase, of the left and right fingers caused by unequal forward and backward friction in the drivetrain. Average speed of the right finger is a little faster than the left, making the object move leftward. It is apparent that large k_c amplifies the chattering, as it allows only small amount of excessive energy to be stored and absorbed. Responses worsen when the objects are pencil eraser and rigid steel plate. k_c of the latter case has increased to 26, 36 N/mm, and a large value associated with soft, stiff, and rigid grippers. Note that $k_c > K_P$ such that stiff environment causes unstable response.

For an egg which represents a brittle and irregular shaped object, rigid gripper creates large overshoot of F_c during the gripping. This induces large contact stress that exceeds ultimate strength of the eggshell, which then is broken at $t = 1.323$ s. On the other hand, the VSP of the hybrid gripper stores and absorbs surplus energy imparted to the egg. Thus, the overshoot is eliminated and the vibration is suppressed dramatically. Moreover, compliance of the VSP makes the pad locally conforms to the curved surface of the egg. Effectively, contact area is enlarged and the stress is reduced. Apparently, the VSP and contact stiffness controller help stabilize robot manipulation in unstructured environment without resorting to intensive planning and control computation.

VI. CONCLUSION

We present a semi-active soft pad called the variable stiffness pad or VSP. It is a uniquely fabricated silicone-based pad of which the stiffness can be modulated through controlling the pressure inside by the customized air compressor unit. In this regard, stiffness model of the VSP is determined experimentally and used for the control. We also propose a concept of hybrid robot that builds upon rigid robot and the attached VSP. Hybrid robot inherits fast and precise motion characteristics of rigid robot as well as safe compliant contact behavior of the VSP. It is capable of performing the tasks in unstructured environment when the manipulation impedance and contact stiffness are tuned properly. Case study of the hybrid gripper picking up different objects is performed. With suitable contact stiffness and gripping force, the hybrid gripper, in contrast with the rigid one, can pick up and place all objects. The VSP is therefore an important ingredient for the robot to interact with various unstructured environment successfully. Its application may be extended further from highly interactive robots such as humanoid and legged robots to prosthesis and rehabilitation robots where patients will benefit more realistic interaction with the environment by additional touch modality.

REFERENCES

[1] W. McMahan, V. Chitrakaran, M. Csencsits, D. Dawson, I. D. Walker, B. A. Jones, M. Pritts, D. Dienno, M. Grissom, and C. D. Rahn, "Field trials and testing of the OctArm continuum manipulator," in *Proc. Int. Conf. Robot. Autom.*, 2006, pp. 2336–2341.

[2] B. Mosadegh, P. Polygerinos, C. Keplinger, S. Wennstedt, R. F. Shepherd, U. Gupta, J. Shim, K. Bertoldi, C. J. Walsh, and G. M. Whitesides, "Pneumatic networks for soft robotics that actuate rapidly," *Adv. Funct. Mater.*, vol. 24, no. 15, pp. 2163–2170, Apr. 2014.

[3] P. Polygerinos, Z. Wang, J. T. B. Overvelde, K. C. Galloway, R. J. Wood, K. Bertoldi, and C. J. Walsh, "Modeling of soft fiber-reinforced bending actuators," *IEEE Trans. Robot.*, vol. 31, no. 3, pp. 778–789, Jun. 2015.

[4] R. K. Katzschmann, C. D. Santina, Y. Toshimitsu, A. Bicchi, and D. Rus, "Dynamic motion control of multi-segment soft robots using piecewise constant curvature matched with an augmented rigid body model," in *Proc. 2nd IEEE Int. Conf. Soft Robot. (RoboSoft)*, Apr. 2019, pp. 454–461.

[5] S. Sanan, "Soft inflatable robots for safe physical human interaction," Ph.D. thesis, Robot. Inst., Carnegie Mellon Univ., Pittsburgh, PA, USA, 2013.

[6] R. Qi, A. Khajepour, W. W. Melek, T. L. Lam, and Y. Xu, "Design, kinematics, and control of a multijoint soft inflatable arm for human-safe interaction," *IEEE Trans. Robot.*, vol. 33, no. 3, pp. 594–609, Jun. 2017.
[7] D. Rus and M. T. Tolley, "Design, fabrication and control of soft robots," *Nature*, vol. 521, no. 7553, pp. 467–475, May 2015.
[8] T. G. Thuruthel, Y. Ansari, E. Falotico, and C. Laschi, "Control strategies for soft robotic manipulators: A survey," *Soft Robot.*, vol. 5, no. 2, pp. 149–163, Apr. 2018.
[9] P. Hyatt, D. Wingate, and M. D. Killpack, "Model-based control of soft actuators using learned non-linear discrete-time models," *Frontiers Robot. AI*, vol. 6, p. 22, Apr. 2019.
[10] J. Bao, W. Chen, and J. Xu, "Kinematics modeling of a twisted and coiled polymer-based elastomer soft robot," *IEEE Access*, vol. 7, pp. 136792–136800, 2019.
[11] P. Ohta, L. Valle, J. King, K. Low, J. Yi, C. G. Atkeson, and Y.-L. Park, "Design of a lightweight soft robotic arm using pneumatic artificial muscles and inflatable sleeves," *Soft Robot.*, vol. 5, no. 2, pp. 204–215, Apr. 2018.
[12] A. Stilli, L. Grattarola, H. Feldmann, H. A. Wurdemann, and K. Althoefer, "Variable stiffness link (VSL): Toward inherently safe robotic manipulators," in *Proc. IEEE Int. Conf. Robot. Autom. (ICRA)*, May 2017, pp. 4971–4976.
[13] S. Joonhigh, N. Kuppuswamy, A. Beaulieu, A. Alspach, and R. Tedrake, "Variable compliance and geometry regulation of soft-bubble grippers with active pressure control," in *Proc. IEEE 4th Int. Conf. Soft Robot. (RoboSoft)*, Apr. 2021, pp. 169–175.
[14] T. Kim, S. J. Yoon, and Y.-L. Park, "Soft inflatable sensing modules for safe and interactive robots," *IEEE Robot. Autom. Lett.*, vol. 3, no. 4, pp. 3216–3223, Oct. 2018.
[15] T. P. Tomo, A. Schmitz, W. K. Wong, H. Kristanto, S. Somlor, J. Hwang, L. Jamone, and S. Sugano, "Covering a robot fingertip with uSkin: A soft electronic skin with distributed 3-axis force sensitive elements for robot hands," *IEEE Robot. Autom. Lett.*, vol. 3, no. 1, pp. 124–131, Jan. 2018.
[16] G. Pang, G. Yang, W. Heng, Z. Ye, X. Huang, H.-Y. Yang, and Z. Pang, "CoboSkin: Soft robot skin with variable stiffness for safer human–robot collaboration," *IEEE Trans. Ind. Electron.*, vol. 68, no. 4, pp. 3303–3314, Apr. 2021.
[17] A. Buso, R. B. N. Scharff, E. L. Doubrovski, J. Wu, C. C. L. Wang, and P. Vink, "Soft robotic module for sensing and controlling contact force," in *Proc. 3rd IEEE Int. Conf. Soft Robot. (RoboSoft)*, May 2020, pp. 70–75.
[18] L. Yao, R. Niiyama, J. Ou, S. Follmer, C. D. Silva, and H. Ishii, "PneUI: Pneumatically actuated soft composite materials for shape changing interfaces," in *Proc. ACM UIST*, Oct. 2013, pp. 13–22.
[19] H. A. Sonar and J. Paik, "Soft pneumatic actuator skin with piezoelectric sensors for vibrotactile feedback," *Frontiers Robot. AI*, vol. 2, p. 38, Jan. 2016.
[20] W. Yuan, S. Dong, and E. Adelson, "GelSight: High-resolution robot tactile sensors for estimating geometry and force," *Sensors*, vol. 17, no. 12, p. 2762, Nov. 2017.
[21] R. Chen, Z. Zhang, J. Guo, F. Liu, J. Leng, and J. Rossiter, "Variable stiffness electroadhesion and compliant electroadhesive grippers," *Soft Robot.*, Dec. 2021, doi: 10.1089/soro.2021.0083.
[22] J. Lai, B. Lu, and H. K. Chu, "Variable-stiffness control of a dual-segment soft robot using depth vision," *IEEE/ASME Trans. Mechatronics*, vol. 27, no. 2, pp. 1034–1045, Apr. 2022.
[23] Blue Danube Robotics GmbH. (Nov. 2021). *AIRSKIN*. [Online]. Available: https://www.airskin.io
[24] FANUC Europe Corporation. (Nov. 2021). *Collaborative Industrial Robot FANUC CR-35iA*. [Online]. Available: https://www.fanuc.eu/be/en/robots/robot-filter-page/collaborative-robots/collaborative-cr35ia
[25] J. Lee, J. Kim, S. Park, D. Hwang, and S. Yang, "Soft robotic palm with tunable stiffness using dual-layered particle jamming mechanism," *IEEE/ASME Trans. Mechatronics*, vol. 26, no. 4, pp. 1820–1827, Aug. 2021.
[26] F.-Y. Xu, F.-Y. Jiang, Q.-S. Jiang, and Y.-X. Lu, "Soft actuator model for a soft robot with variable stiffness by coupling pneumatic structure and jamming mechanism," *IEEE Access*, vol. 8, pp. 26356–26371, 2020.
[27] C. An and J. Hollerbach, "Dynamic stability issues in force control of manipulators," in *Proc. IEEE Int. Conf. Robot. Autom.*, Mar. 1987, pp. 890–896.
[28] E. Colgate and N. Hogan, "An analysis of contact instability in terms of passive physical equivalents," in *Proc. Int. Conf. Robot. Autom.*, 1989, pp. 404–409.
[29] W. S. Newman, "Stability and performance limits of interaction controllers," *J. Dyn. Syst., Meas., Control*, vol. 114, no. 4, pp. 563–570, 1992.
[30] D. C. Karnopp, D. L. Margolis, and R. C. Rosenberg, *System Dynamics: Modeling, Simulation, and Control of Mechatronic Systems*, 5th ed. Hoboken, NJ, USA: Wiley, 2012.
[31] D. Ratna and J. Karger-Kocsis, "Recent advances in shape memory polymers and composites: A review," *J. Mater. Sci.*, vol. 43, no. 1, pp. 254–269, Jan. 2008.
[32] C. Cheng, J. Cheng, and W. Huang, "Design and development of a novel SMA actuated multi-DOF soft robot," *IEEE Access*, vol. 7, pp. 75073–75080, 2019.
[33] A. O'Halloran, F. O'Malley, and P. McHugh, "A review on dielectric elastomer actuators, technology, applications, and challenges," *J. Appl. Phys.*, vol. 104, no. 7, 2008, Art. no. 071101.
[34] Y. Sun, Y. S. Song, and J. Paik, "Characterization of silicone rubber based soft pneumatic actuators," in *Proc. IEEE/RSJ Int. Conf. Intell. Robots Syst.*, Nov. 2013, pp. 4446–4453.
[35] G. P. Horedt, *Polytropes: Applications in Astrophysics and Related Fields*. Dordrecht, The Netherlands: Kluwer, 2004. [Online]. Available: https://www.nhbs.com/publisher/kluwer?q=&dFR[publisher.name][0]=Kluwer%20Academic%20Publishers&fR[doc_s][0]=false&fR[hide][0]=false&fR[live][0]=true
[36] G. J. V. Wylen, R. E. Sonntag, and C. Borgnakke, *Fundamentals of Classical Thermodynamics*, 4th ed. Hoboken, NJ, USA: Wiley, 1994.
[37] J. J. E. Slotine and S. S. Sastry, "Tracking control of nonlinear systems using sliding surfaces with application to robot manipulators," *Int. J. Control*, vol. 38, no. 2, pp. 465–492, 1983.
[38] A. H. Khan and S. Li, "Sliding mode control with PID sliding surface for active vibration damping of pneumatically actuated soft robots," *IEEE Access*, vol. 8, pp. 88793–88800, 2020.
[39] B. Siciliano, L. Sciavicco, L. Villani, and G. Oriolo, *Robotics: Modelling, Planning, and Control*. London, U.K.: Springer-Verlag, 2010.

PHONGSAEN PITAKWATCHARA received the B.Eng. degree (summa cum laude) from Chulalongkorn University, Thailand, in 1997, the M.S.M.E. degree from the Georgia Institute of Technology, USA, in 2000, and the Ph.D. degree from The University of Tokyo, Japan, in 2007, all in mechanical engineering.

Since then, he has been affiliated with the Department of Mechanical Engineering, Chulalongkorn University, where he is currently an Associate Professor. His research interests include telerobotics, haptics, flexible robots, soft robots, robot manipulation and planning, redundant robots, intelligent robots, dynamics and control of robotic, and mechatronic systems.

JETNIPIT ARUNRAT received the B.Eng. and M.Eng. degrees in mechanical engineering from Chulalongkorn University, in 2018 and 2022, respectively. His research interests include human-robot interaction, impedance control, force control, soft robots, and soft actuators.